Correlated states in a model two-dimensional layer

D. Denley and L. M. Falicov
Department of Physics, University of California, Berkeley, California 94720*
(Received 7 September 1977)

We present results of a calculation to model the behavior of density-wave correlated states in layered compounds of the trigonal prismatic type. The effect of an attractive or repulsive intrasite interaction between itinerant electrons is studied in the Hartree-Fock approximation for a two-dimensional band structure. The stable state depends on the electron-electron interaction parameter and it may be (i) the normal paramagnetic state, (ii) the ferromagnetic state, (iii) a single charge-density wave, (iv) a single spin-density wave, (v) a triple charge-density wave, (vi) a novel asymmetric charge-density wave, or (vii) a mixed state which shows spin and charge-density waves for *repulsive* electron-electron interactions. The solutions are characterized by a generalized conductivity.

I. INTRODUCTION

In 1960 Overhauser[1,2] suggested that the paramagnetic state of a gas of interacting fermions is unstable to the formation of spin-density waves (SDW) or charge-density waves (CDW, DW collectively). In the formation of a density wave the electrons correlate so that the electron density for a spin shows a new periodicity

$$\rho_\sigma(\vec{r}) = a\,[1 - \phi\cos(\vec{Q}^* \cdot \vec{r} - \alpha)]\,.$$

In the CDW, the spin-up and spin-down density waves are the same so there is nowhere a net magnetization. For the SDW the two density waves have opposite phase so that while the total charge density is uniform, there is a wave of magnetization. In general intermediate states are possible.

Interest in density waves has intensified recently as a variety of materials now seem to show density-wave behavior. Chromium[3-7] provided much of the early interest as an example of an itinerant antiferromagnet (SDW). Recently,[8-12] the quasi-one-dimensional compounds tetrathiafulvalene-tetracyanoquinodimethane and $NbSe_3$ have been shown to exhibit charge-density waves. Another class of materials are of interest because of their anomalous electronic properties: the layered transition-metal dichalcogenides.[13-17] Wilson *et al.*[15] have shown that CDW formation is the source of the periodic lattice displacements for these materials and that these DW correlations occur in three symmetry related directions simultaneously to form a triple charge-density wave (TCDW). It has been proposed that a mechanism that leads to DW formation in the $1T$ polytypes is related to a specific nesting character of the Fermi surface.

More recently, Rice and Scott[18] have noted that the generalized susceptibility $\chi(\vec{q})$ of two-dimensional materials that have two or more saddle points in their band structure can diverge. The divergence occurs if the Fermi level approaches both saddle points and it is exhibited in χ for wave vectors $\vec{Q}_\alpha^*$ connecting the saddle points. This divergence signals that the paramagnetic ground state should be unstable to DW fluctuations of wave vector $\vec{Q}_\alpha^*$. The detailed nature of the ground state is not obtainable by this susceptibility calculation. A more complete model should go further to include finite amplitude effects, as well as the symmetry of the system.

It is our purpose to solve a simple two-dimensional model that incorporates the lattice symmetry and a nontrivial Fermi surface and to characterize the properties of the resulting solutions.

The transition-metal dichalcogenides show a structure in which triple XMX layers are held together mainly by Van der Waals forces.[15] Each XMX layer consists of three hexagonally packed atomic planes; one metal plane M is surrounded by two planes of chalcogen X atoms. An atom of the metal atomic plane can find itself in either trigonal prismatic or octahedral coordination with the surrounding chalcogens. The various methods of stacking the layers give rise to a large variety of "polytypes." Our parameters were chosen to reflect a single layer of these materials.

II. THE MODEL

Because of their conductivity behavior,[15,19] the transition-metal dichalcogenides can be regarded as quasi-two-dimensional. We feel that since conductivity takes place mainly through the metal orbitals, it would suffice to take a model of a single band of states arising from a layer of metal atoms. The band parameters are chosen so as to copy the main features (maxima, minima, and saddle points) of the single band at the Fermi level in the so-called $2H$ polytype of $NbSe_2$, as calculated by Mattheiss using the augmented-plane-

wave method.[20] We made slight alterations to set the Fermi level to coincide with the saddle point at the T point, exactly halfway between Γ and K. Since an instability is expected to set in for wave vectors connecting the saddle points, we have altered the bands slightly so that $\vec{Q}_\alpha^* = \frac{1}{2}\vec{G}$, where $\vec{G}$ is a particular vector of the reciprocal lattice. In this way the DW's will be in a commensurate state. The paramagnetic Fermi surface is shown in Fig. 1. It corresponds to 0.74 electrons per chemical unit cell, i.e., the Fermi surface occupies 0.37 of the original Brillouin zone (BZ). The itinerant-electrons effective Hamiltonian[3,21,22] is given by

$$\mathcal{H} = \sum_{i,j,\sigma} t_{ij} a_{i\sigma}^\dagger a_{j\sigma} + U \sum_i n_{i\uparrow} n_{i\downarrow} . \tag{1}$$

The $a_{i\sigma}^\dagger$ and $a_{i\sigma}$ are the creation and destruction operators of the tight-binding Wannier states for site i and spin σ. The t_{ij} are the hopping parameters between atoms i and j, so the band energy is

$$\epsilon_{\vec{k}} = N^{-1} \sum_j e^{i\vec{k}\cdot(\vec{R}_i - \vec{R}_j)} t_{ij} .$$

Our model contains hopping out to the fifth nearest neighbor. The model includes only short-range interactions, i.e., Coulomb interactions for electrons only in the same cell.

We solved the Schrödinger equation for the above Hamiltonian in the unrestricted Hartree-Fock approximation. The equivalent Hartree-Fock Hamiltonian in the Bloch basis is then

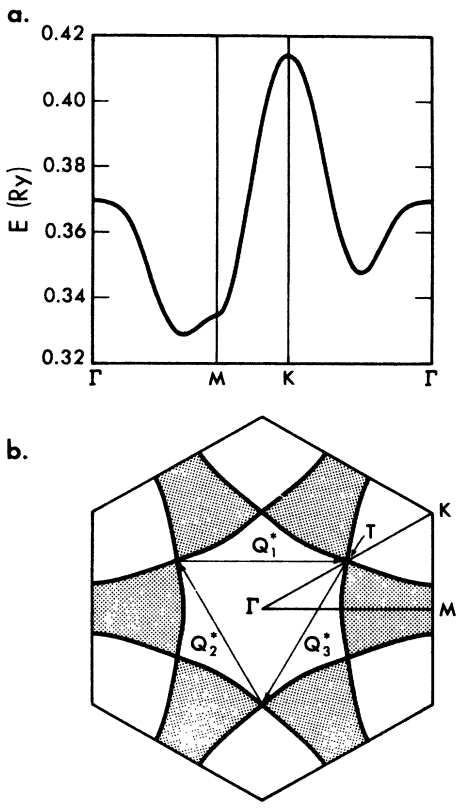

FIG. 1. (a) Six-parameter fit to the conduction band in 2H-$NbSe_2$ as calculated by Mattheiss. The displacement in the bottom of the band is an artificial result in improving the curvature of the Fermi surface. (b) Fermi surface with the wave vectors and the symmetry points of the BZ indicated.

$$\mathcal{H}_{SCF} = \sum_{\vec{k},\sigma} \epsilon_{\vec{k}} a_{\vec{k}\sigma}^\dagger a_{\vec{k}\sigma} + \frac{U}{N} \sum_{\vec{Q}} \sum_{\vec{k}\,\vec{k}'} [\langle a_{\vec{k}+\vec{Q}\uparrow}^\dagger a_{\vec{k}\uparrow}\rangle a_{\vec{k}'-\vec{Q}\downarrow}^\dagger a_{\vec{k}'\downarrow} + \langle a_{\vec{k}'-\vec{Q}\downarrow}^\dagger a_{\vec{k}'\downarrow}\rangle a_{\vec{k}+\vec{Q}\uparrow}^\dagger a_{\vec{k}\uparrow} - \langle a_{\vec{k}+\vec{Q}\uparrow}^\dagger a_{\vec{k}\uparrow}\rangle \langle a_{\vec{k}'-\vec{Q}\downarrow}^\dagger a_{\vec{k}'\downarrow}\rangle$$
$$- \langle a_{\vec{k}+\vec{Q}\uparrow}^\dagger a_{\vec{k}'\downarrow}\rangle a_{\vec{k}'-\vec{Q}\downarrow}^\dagger a_{\vec{k}\uparrow} - \langle a_{\vec{k}'-\vec{Q}\downarrow}^\dagger a_{\vec{k}\uparrow}\rangle a_{\vec{k}+\vec{Q}\uparrow}^\dagger a_{\vec{k}'\downarrow} + \langle a_{\vec{k}+\vec{Q}\uparrow}^\dagger a_{\vec{k}'\downarrow}\rangle \langle a_{\vec{k}'-\vec{Q}\downarrow}^\dagger a_{\vec{k}\uparrow}\rangle] . \tag{2}$$

We only consider solutions for which the correlation functions

$$\delta_{\vec{Q}\sigma\sigma'} = N^{-1} \sum_{\vec{k}} \langle a_{\vec{k}+\vec{Q}\sigma}^\dagger a_{\vec{k}\sigma'}\rangle$$

are nonzero only for $\sigma = \sigma'$, and $\vec{Q} = \vec{Q}_\alpha^*$ and $\vec{Q} = 0$. We thus exclude solutions for which the last three terms in (2) contribute.

For general $\vec{Q}$, incommensurate with the lattice, the gap parameters $\Delta_{\vec{Q}\sigma} = U\delta_{\vec{Q}\sigma}$, connects any state of spin σ with an infinity of other states. But if the $\vec{Q}$ is an integral fraction of some reciprocal-lattice vector, i.e., commensurate with the lattice, the set of connected states close and the system displays a new periodicity to which Bloch's theorem can be applied. In the model we are considering there are four states interacting and the new, reduced BZ is one fourth the original size [Fig. 2(a)]. At this point it is more convenient to relabel the original unmixed Bloch states $\vec{k}$ by a reduced wave vector $\vec{k}$ and "band" index $\eta = 1, 2, 3, 4$. The new folded paramagnetic band structure is shown in Fig. 2(b). The Hamiltonian matrix takes now the form

$$\begin{bmatrix} \epsilon_{\vec{k},\eta_1} + Un_\sigma & \Delta_{1\sigma} & \Delta_{2\sigma} & \Delta_{3\sigma} \\ \Delta_{1\sigma} & \epsilon_{\vec{k},\eta_2} + Un_\sigma & \Delta_{3\sigma} & \Delta_{2\sigma} \\ \Delta_{2\sigma} & \Delta_{3\sigma} & \epsilon_{\vec{k},\eta_3} + Un_\sigma & \Delta_{1\sigma} \\ \Delta_{3\sigma} & \Delta_{2\sigma} & \Delta_{1\sigma} & \epsilon_{\vec{k},\eta_4} + Un_\sigma \end{bmatrix} \tag{3}$$

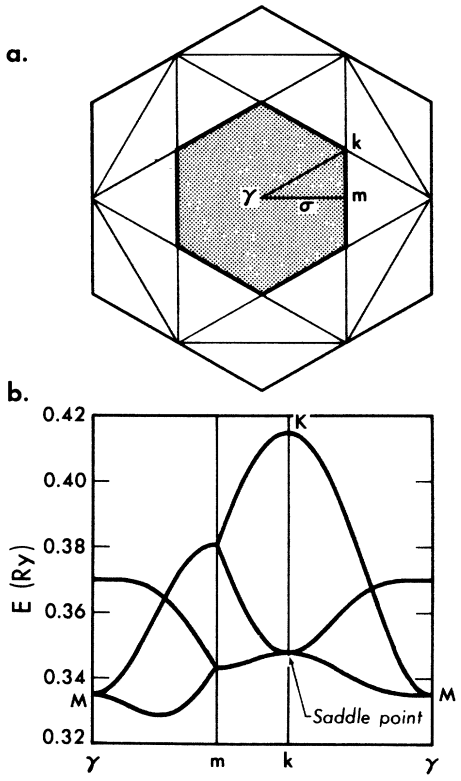

FIG. 2. (a) Folded BZ in the extended-zone scheme. (b) Folded band structure.

where

$$n_\sigma = \delta_{\vec{Q}=0,\sigma} = N^{-1} \sum_{\vec{k}} \langle a^\dagger_{\vec{k}\sigma} a_{\vec{k}\sigma} \rangle$$

is just the average number density for spin σ.

The Hartree-Fock equations were solved by an iterative procedure. An initial approximation for the $\delta_{\vec{Q}\sigma}$ is used in Eq. (3). If the eigenstates of the approximate Hartree-Fock Hamiltonian are labeled $|\vec{k}\lambda\sigma\rangle$, where λ is the new band index, then the correlation function can be calculated by

$$\delta_{\vec{Q}\sigma} = N^{-1} \sum_{\vec{k},\eta,\lambda} f_{\vec{k}\lambda\sigma} \langle \vec{k}\eta'\sigma | \vec{k}\lambda\sigma \rangle \langle \vec{k}\lambda\sigma | \vec{k}\eta\sigma \rangle , \quad (4)$$

where there is, for each k vector, a unique one-to-one correspondence between the band indices η and η' and the Q vector connecting any two relevant states; $f_{\vec{k}\lambda\sigma}$ is the Fermi factor. The values of $\Delta_{\vec{Q}\sigma}$ resulting from (4) are inserted into (3) and the process is repeated until self-consistency is obtained. In our calculations the unfolded BZ was covered with a grid of 1200 points. The state can be characterized by calculating the site density of electrons

$$\rho_\sigma(\vec{r}) = \sum_{\vec{Q}} \delta_{\vec{Q}\sigma} \cos(\vec{Q}\cdot\vec{r}) .$$

While convergence was good for $|U|$ either small or large compared to the overall paramagnetic bandwidth B, the convergence was often slow in the intermediate regime $|U| \approx B$. Solutions were found for the cases of both attractive and repulsive U. Several states were studied in each regime and a phase diagram of total energy per electron (E_T/N_e) as a function of U was calculated.

One point is worth considering. The band structure given in Figs. 1 and 2 contains, as all two-dimensional structures, logarithmic singularities due to the saddle points. These do appear in the density-of-states and in the susceptibility calculations. These logarithmic singularities are by necessity extremely weak and the numerical procedures used in this paper are not sensitive enough to produce the corresponding divergences in the relevant quantities. In this sense our real band structure is not the continuous curve depicted in Figs. 1 and 2, but rather the collection of 1200 points chosen in the grid used in our numerical procedures.

It should also be pointed out that we are not concerned with instability (susceptibility) calculations, but with total-energy values. Since typical energy gaps are of the order of 10^{-3} Ry, our error in total energies due to our numerical approximations in the vicinity of the saddle point can be estimated to be less than 10^{-4} Ry per electron. This should be kept in mind when analyzing our results.

III. RESULTS

There were several types of solution that were studied: (a) The simplest is the paramagnetic state (P) in which the single-particle band is doubly occupied according to Fermi statistics. (b) The ferromagnetic case (F) in which the band is filled with electrons of mainly one spin. (c) The CDW which has correlations for a single $\vec{Q}^*_\sigma$ only. (d) The TCDW, which has the full symmetry of the lattice and has correlations in the three symmetry-related $\vec{Q}^*_\sigma$'s simultaneously. (e) The asymmetric charge-density wave (ACDW) which has correlations in the three $\vec{Q}^*_\sigma$ but of different amplitudes so that the resulting state is of low symmetry. (f) The SDW which only differs from CDW in the phase of the waves of opposite spin. (g) A mixed density wave (MDW) which has the full hexagonal symmetry of TCDW, but it has correlations in charge *and* spin. Further details are summarized in Table I.

Some of the physical limits should be noted. As $U \to 0$ it is obvious that the paramagnetic state is stable. At the opposite extremes, $U \to \pm\infty$, the value of the electron density becomes the most important parameter. In the attractive atomic limit ($U \to -\infty$)

TABLE I. Characterization of the various states.

	Degree	Atoms per cell	Symmetry	Δn	$\delta_{1\uparrow}$	$\delta_{2\uparrow}$	$\delta_{3\uparrow}$	$\delta_{1\downarrow}$	$\delta_{2\downarrow}$	$\delta_{3\downarrow}$
Paramagnetic (P)	0	1	D_{6h}	0	0	0	0	0	0	0
Charge-density wave (CDW)	1	2	D_{2h}	0	a	0	0	a	0	0
Triple charge-density wave (TCDW)	1	4	D_{6h}	0	a	a	a	a	a	a
Asymmetric charge-density wave (ACDW)	2	4	S_2	0	a	a	b	a	a	b
Ferromagnetic (F)	1	1	D_{6h}	a	0	0	0	0	0	0
Spin-density wave (SDW)	1	2	D_{2h}	0	a	0	0	$-a$	0	0
Mixed-density wave (MDW)	3	4	D_{6h}	a	b	b	b	c	c	c

electrons always try to pair up on a site, while for the repulsive case electrons try to avoid being at the same site. If we consider $n=\frac{3}{4}$ (which is approximately our value of $n=0.74$) the smallest unit cell containing an integral number of electrons would be a 2×2 or 4×1 structure. However, in the attractive atomic limit, a lower energy is obtained with an eight-atom unit cell that contains an even integral number of electrons. This allows for several states with complete site pairing. For repulsive U, a four-atom unit cell is sufficient to minimize the energy. While the simplest state one can construct to minimize the energy is ferromagnetic, there is a large number of other possible states that have no site pairing and derive from antiferromagnetic states. To get a clear picture of the most stable state, one must do perturbation theory in the bandwidth (B/U) to find the stable state. For other n, very large unit cells become possible.

In principle one could also calculate a Landau phase diagram in which energy is given as a function of the relevant order parameters. It is apparent that for our model there are, in general, seven order parameters: six $\Delta_{Q\sigma}$ and $\Delta n = n_\uparrow - n_\downarrow$, so that a complete Landau diagram cannot be easily visualized. At the same time, no stable solution with more than three independent order parameters has been found. This number is given as the "degree" of the state in Table I. With these preliminaries completed we can discuss the solutions in detail. For clarity, most of the states are also illustrated in Fig. 3.

A. Paramagnetism

The paramagnetic solution exists for all U. In the band structure of Figs. 1 and 2, since the Fermi level E_F is placed at the saddle points, the density of states N_F at the Fermi level and $\chi(Q_\sigma^*)$ diverge so that P is only stable for $U=0$. However, in the numerical calculations,[23] the two quantities become finite so that P is stable for a range of small U. The total energy of P is simply

$$E_T = E_B + UN_e^2/4N,$$

where

$$E_B = \sum_{\vec{k},\sigma} f_{\vec{k}} \epsilon_{\vec{k}}$$

and

$$N_e = nV,$$

and N is the number of atoms.

B. Charge-density wave

The CDW is characterized by one nonzero correlation function $\delta = \delta_{\vec{Q}^*\uparrow} = \delta_{\vec{Q}^*\downarrow}$ for only one of the

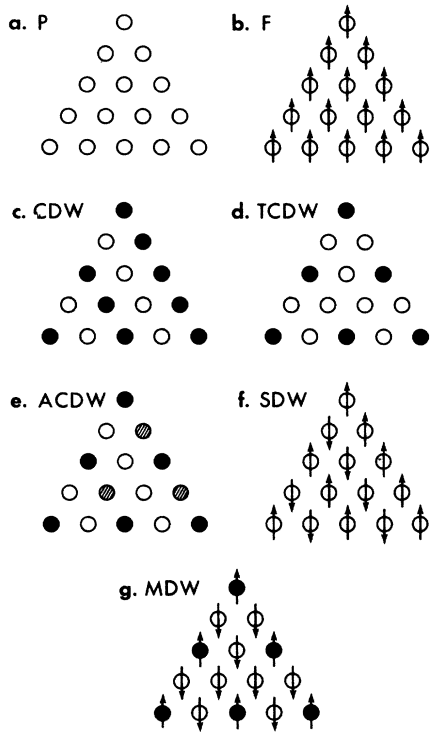

FIG. 3. Real-space depiction of the self-consistent states. In all these diagrams open circles are sites of low density, closed circles are high density, shaded circles indicate intermediate density. (a) Real-space lattice; (b) F; (c) CDW; (d) TCDW; (e) ACDW; (f) SDW; (g) MDW.

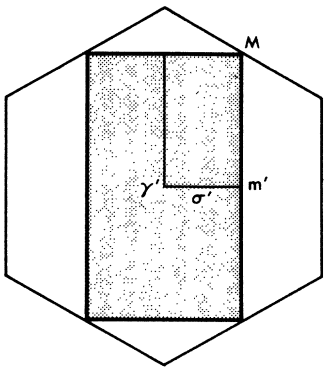

FIG. 4. BZ for the single charge-density and spin-density wave states.

three vectors $\vec{Q}_\alpha^*$. This causes the CDW to break the point-group symmetry and yield a rectangular unit cell with two atoms, with the BZ shown in Fig. 4. The relationship of the rectangular BZ of Fig. 4 to the basic one of Fig. 2(a) is evident. Since the three $\vec{Q}_\alpha^*$ are equivalent, there are three equivalent CDW states and microscopic domains might coexist. The CDW exists for $U<-0.28B$. However, up to $U\approx-0.35B$ there is a multiplicity of CDW solutions (see Fig. 5). The values are such

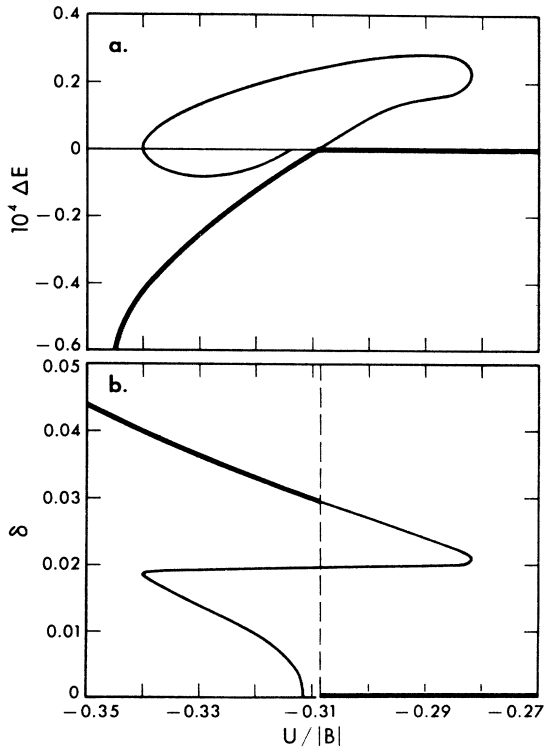

FIG. 5. Behavior of CDW near its transition point. (a) Energy is measured with respect to the paramagnetic energy, $\Delta E=[E_T(\mathrm{CDW})-E_T(P)]/N_e|B|$. (b) Variation of δ vs $U/|B|$.

that the transition to P is discontinuous (1st order phase transition) as a function of U.

C. Triple charge-density wave

The TCDW has one order parameter $\delta_{i\sigma}=\delta_t$ for all i,σ, so that the state has the full hexagonal symmetry with a unit cell of four atoms. From (5) above the electron density for spin σ breaks into a three-and-one structure; three atoms with density $n_\sigma-\delta_t$ and one with $n_\sigma+3\delta_t$, where in our case only $\delta_t>0$ appears. The TCDW state exists for $U<-0.29B$. The transition to P as a function of U is continuous (second-order transition).

D. Asymmetric-density wave

The ACDW has two independent order parameters that yield a four-atom unit cell and allows only inversion symmetry. For particular limits, the order parameters become identical to those for either TCDW or CDW. In the ACDW state, one site is highly populated, two have low populations and the fourth is of intermediate value. While for large U, ACDW is unique, for $U\gtrsim-0.62B$ there are two solutions, one resembling a single CDW and the other resembling TCDW. In fact they do merge into those states at $U=-0.35B$ approximately. These ACDW→CDW and ACDW→TCDW transitions are second-order within the accuracy of our calculations. The relationships between the order parameters of CDW, TCDW, and ACDW are illustrated in Fig. 6. There are three equivalent ACDW's, one for each value of $\vec{Q}_\alpha^*$, as a consequence, three types of domain may exist. Figure 6 can also be looked at as one that provides a measurement of the instability of the CDW against the formation of ACDW, i.e., the tendency towards the formation of a multiple density wave.

E. Ferromagnetism

As with P, F has hexagonal symmetry and a unit cell of one atom but the spin symmetry is broken. With ferromagnetic occupation the one electron band for one spin contains more electrons than the other. This state may only exist for repulsive U. If U is not large enough, the state becomes unstable against the transfer of electrons from the top of the majority band to the lowest unoccupied state in the minority band. This entails a decrease in the magnetization and in fact it is necessary to minimize E_T with respect to the magnetization M for given U. We find a second order transition of F to a partially ferromagnetic state at $U=0.61B$ and then a first order phase transition for $M/N_e=0.081$ to 0 at $U=0.34B$. This is illustrated in Fig. 7.

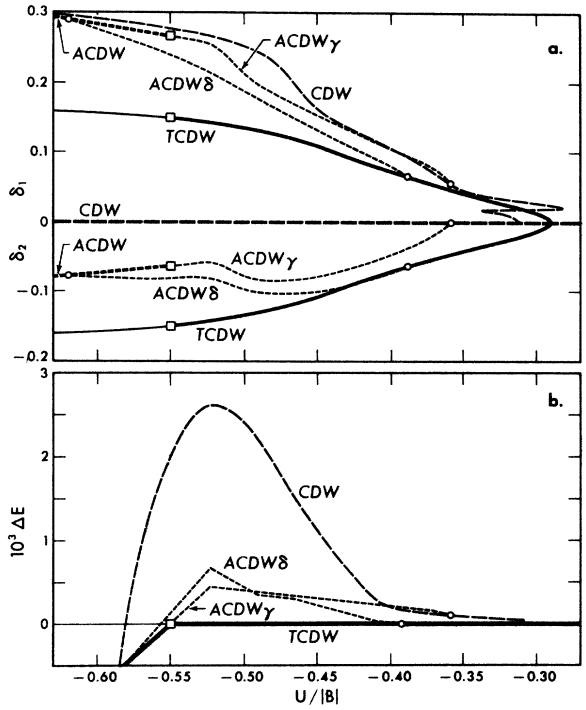

FIG. 6. Relationship of ACDW to CDW and TCDW for small $U/|B|$. The ACDW state has two order parameters δ_1, δ_2. For the CDW state $\delta_1 = 0$ always, and for the TCDW state $\delta_1 = \delta_2$ always. (a) Plot of δ_1 vs $U/|B|$ (upward) and δ_2 vs $U/|B|$ (downward). (b) Plot of $\Delta E \equiv [E_T - E_T(\mathrm{TCDW})]/N_e|B|$ vs $U/|B|$. ACDWγ and ACDWδ represent two different solutions.

F. Spin-density wave

For any U in which there is a CDW solution, there is a SDW state existing at $(-U)$ with the same DW amplitude in magnitude but $\delta_{\vec{Q}\uparrow} = -\delta_{\vec{Q}\downarrow}$ so that the peak in the wave for one spin falls on the trough of the other. Once again the hexagonal symmetry is broken and the solution becomes multiply valued for small U, resulting in a first-order transition to P. Figure 5 is the corresponding graph if $U \to -U$.

G. Mixed-density wave

The MDW state depends crucially on the number of electrons and in our model exists only for $\frac{1}{4} \leq n \leq \frac{3}{4}$. In the MDW one of the spin bands is preferentially occupied and there are two symmetric triple-density waves, one for each spin. These involve the same three $\vec{Q}_\alpha^*$ vectors but have different amplitudes for each spin. The majority spin mainly populates one site of a four atom unit cell and more weakly the other three, while the minority spin populates mainly the last three sites. The result is that MDW exhibits SDW and CDW behavior together with a net magnetization. Because of the full hexagonal symmetry of the spatial arrangement and the breaking of the spin symmetry, the total symmetry is the same as F but with a larger unit cell. The three order parameters decrease with U, down to $U \approx 0.29B$, where a transition to P occurs that is second order to within the accuracy of our calculation.

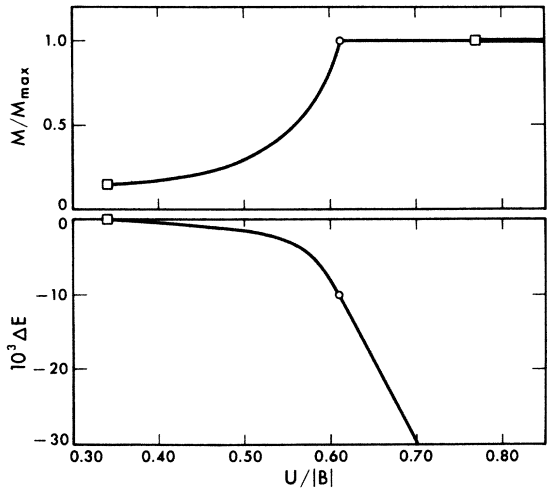

FIG. 7. Behavior of F. The upper graph gives the net magnetization $M/M_{\max} \equiv (n\uparrow - n\downarrow)/(n\uparrow + n\downarrow)$ as a function of $U/|B|$. The lower graph is a plot of $\Delta E \equiv [E_T(F) - E_T(P)]/N_e|B|$ vs $U/|B|$.

H. Phase diagram

Figure 8 illustrates the stable states and the regions in which they are stable. From the attractive atomic limit $U \to -\infty$ to $U = -0.56B$, ACDW is stable. For $-0.56B < U < -0.47B$ there is a crossover region in which the ordering of the three most-stable DW states completely reverses and

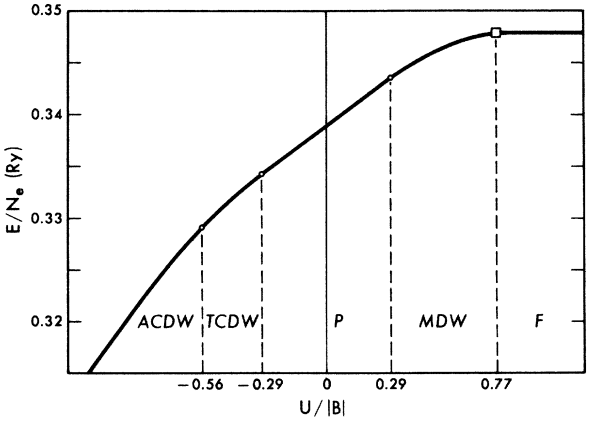

FIG. 8. Phase diagram for the states for both attractive and repulsive U. Circles indicate second-order (continuous) transitions; squares represent first-order (discontinuous) transitions.

during which their energies are quite close. Nonetheless TCDW remains stable after a second-order transition from ACDW and up to $U=-0.29B$. There is, at this point, a second-order transition to P which is stable for the remaining range of attractive interactions. The state P remains stable for repulsive U up to $U=0.29B$, where there is a second-order transition to MDW. The state MDW is stable up to $U=0.77B$ at which point there is a 1st order phase transition to F. The pure ferromagnetic state then remains stable to the atomic limit $U\to\infty$.

I. Generalized conductivity

We have also calculated a generalized conductivity tensor in the basal plane by means of the formula

$$\sigma_{ij}=\sum_{\text{spin}}\frac{m_e}{(2\pi)^2\hbar n}\int_{\text{Fermi surface}}\frac{v_i v_j}{|\vec{v}|}dS\,,$$

where v_i is the band velocity

$$v_i=\hbar^{-1}\frac{\partial\epsilon_{\vec{k}}}{\partial k_i}\,.$$

This formula does not include scattering time effects and it only gives information about the dynamics of electrons, i.e., their velocity and availability of phase space.[24]

All states showed a qualitatively similar behavior. The magnitude of the $\sigma_{ij}(P)$ is the largest generally and the other states start with small values for large U. This is typical and reflects electron localization and band narrowing in the atomic regime. As $|U|$ decreases, σ_{xx} and σ_{yy} increase to values similar to those of the paramagnetic state. Rice and Scott[18] have pointed out that the electrons at the saddle points may be especially effective in electron-electron scattering so that their removal from opening a gap might actually increase the conductivity; our calculation does not exhibit the predicted increase in σ.

IV. SUMMARY

In this work we have tried to characterize more fully those states that should be of importance to the study of electron correlated density-wave states in hexagonal layers. Of necessity the model contained significant simplifications, and the exact relations of stability can be sensitive to details of the band structure. However we feel that the actual stability relations in the $2H$ layer materials are similar and that the essential nature of the states investigated is accurate.

In addition, some results have supplied new details to the theory of charge-density waves in layer compounds, while other results are distinctly novel. If the effective intrasite quasiparticle interaction is attractive, an ACDW is quite possibly the ground state.

It is worth noting that if the actual band structure and the placement of the Fermi level are found to be favorable (so $n_e\approx\frac{2}{9}m$, m is an integer having no common divisors with 9) we can expect that an ACDW on a 3×3 supercell will show two types of site. There would be m sites that are nearly full; and $9-m$ sites that are nearly empty. This state would explain the NMR experiments of Ehrenfreund *et al.*[25] which the TCDW cannot do. Alternatively, for a repulsive effective intrasite interaction a MDW is stable in a wide region and shows a strong triple charge-density wave amplitude that arises in a natural way from the symmetry of the system.

---

*Work supported in part by the NSF through Grant No. DMR76-80561.

[1]A. W. Overhauser, Phys. Rev. Lett. 4, 415 (1960).
[2]A. W. Overhauser, Phys. Rev. 128, 1437 (1962).
[3]D. R. Penn, Phys. Rev. 142, 350 (1966).
[4]P. A. Fedders and R. C. Martin, Phys. Rev. 143, 245 (1966).
[5]A. Arrott, S. A. Werner, and H. Kendrick, Phys. Rev. Lett. 14, 1022 (1965).
[6]A. S. Barker, Jr., B. I. Halperin, and T. M. Rice, Phys. Rev. Lett. 20, 384 (1968).
[7]W. M. Lomer, Proc. Phys. Soc. Lond. 84, 327 (1964).
[8]H. R. Zeller, in *Low-Dimensional Cooperative Phenomena*, edited by H. J. Keller (Plenum, New York, 1975), pp. 215–223; and A. J. Heeger and A. F. Garito, *ibid.*, pp. 89–123.
[9]F. Denoyer, R. Comès, A. F. Garito, and A. J. Heeger, Phys. Rev. Lett. 35, 445 (1975).
[10]S. Kagoshima, H. Anzai, K. Kajimura, and T. Ishiguro, J. Phys. Soc. Jpn. 39, 1143 (1975).
[11]R. Comès, S. M. Shapiro, G. Shirane, A. F. Garito, and A. J. Heeger, Phys. Rev. Lett. 35, 1518 (1975).
[12]P. Monceau, N. P. Ong, A. M. Portis, A. Meershaut, and J. Rouxel, Phys. Rev. Lett. 37, 602 (1976).
[13]D. E. Moncton, J. D. Axe, and F. J. DiSalvo, Phys. Rev. Lett. 34, 734 (1975).
[14]J. A. Wilson, F. J. DiSalvo, and S. Mahajan, Phys. Rev. Lett. 32, 882 (1974).
[15]J. A. Wilson, F. J. DiSalvo, and S. Mahajan, Adv. Phys. 24, 117 (1975).
[16]W. L. McMillan, Phys. Rev. B 12, 1187 (1975).
[17]W. L. McMillan, Phys. Rev. B 12, 1197 (1975).
[18]T. M. Rice and G. K. Scott, Phys. Rev. Lett. 35, 120 (1975).
[19]W. J. Wattamaniuk, J. P. Tidman, and R. F. Frindt, Phys. Rev. Lett. 35, 62 (1975).
[20]L. F. Mattheiss, Phys. Rev. B 8, 3719 (1973); see

also, G. Wexler and A. M. Woolley, J. Phys. C 9, 1185 (1976).
[21]J. Hubbard, Proc. R. Soc. Lond. A 276, 238 (1963).
[22]J. C. Kimball, Phys. Rev. 183, 533 (1969).
[23]Density-wave states exist for all U, but only for a Fermi level *exactly* at the logarithmic singularity in the density of states. Even in this case, in the range of parameters for which our numerical calculations yield a stable P, the difference in energy between paramagnetic and density-wave solutions is less than 10^{-4} Ry per electron.
[24]Anisotropic effects in the electron scattering may produce a change in the measured conductivity above and beyond the effects reported here. See, for example, V. F. Gantmakher and V. A. Gasparov, Zh. Eksp. Teor. Fiz. 64, 1712 (1973) [Sov. Phys.-JETP 37, 864 (1973)]. These considerations are outside the scope of the present investigation. It is unlikely, however, that anistropy of scattering times can reconcile our calculation with Rice and Scott's speculation.
[25]E. Ehrenfreund, A.C. Gossard, F. R. Gamble, and T. H. Geballe, J. Appl. Phys. 42, 1419 (1971).

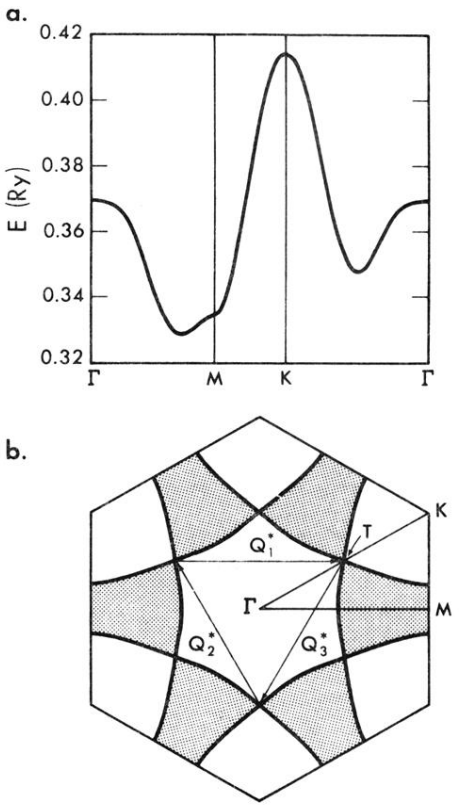

FIG. 1. (a) Six-parameter fit to the conduction band in 2 H-$NbSe_2$ as calculated by Mattheiss. The displacement in the bottom of the band is an artificial result in improving the curvature of the Fermi surface. (b) Fermi surface with the wave vectors and the symmetry points of the BZ indicated.

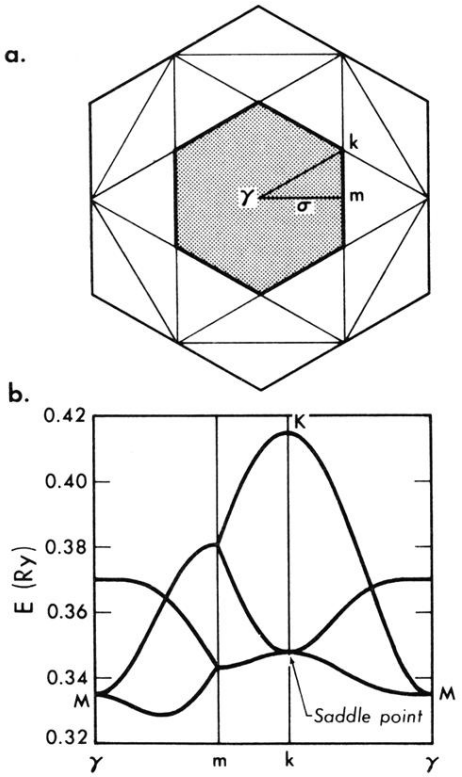

FIG. 2. (a) Folded BZ in the extended-zone scheme.
(b) Folded band structure.

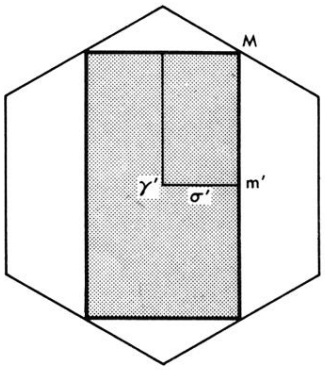

FIG. 4. BZ for the single charge-density and spin-density wave states.